The HCUAV project: Electronics and software development for medium altitude remote sensing

A. Amanatiadis*, E. G. Karakasis*, L. Bampis*, T. Giitsidis†, P. Panagiotou‡,
G. Ch. Sirakoulis†, A. Gasteratos*, Ph. Tsalides†, A. Goulas‡, and K. Yakinthos‡

*Department of Production and Management Engineering, Democritus University of Thrace, GR-67100, Xanthi, Greece
†Department of Electrical and Computer Engineering, Democritus University of Thrace, GR-67100, Xanthi, Greece
‡Department of Mechanical Engineering, Aristotle University of Thessaloniki, GR-54124, Thessaloniki, Greece

***Abstract*—The continuous increase of illegal migration flows to southern European countries has been recently in the spotlight of European Union due to numerous deadly incidents. Another common issue that the aforementioned countries share is the Mediterranean wildfires which are becoming more frequent due to the warming climate and increasing magnitudes of droughts. Different ground early warning systems have been funded and developed across these countries separately for these incidents, however they have been proved insufficient mainly because of the limited surveyed areas and challenging Mediterranean shoreline and landscape. In 2011, the Greek Government along with European Commission, decided to support the development of the first Hellenic Civil Unmanned Aerial Vehicle (HCUAV), which will provide solutions to both illegal migration and wildfires. This paper presents the challenges in the electronics and software design, and especially the under development solutions for detection of human and fire activity, image mosaicking and orthorectification using commercial off-the-shelf sensors. Preliminary experimental results of the HCUAV medium altitude remote sensing algorithms, show accurate and adequate results using low cost sensors and electronic devices.**

I. Introduction

Unmanned airborne remote sensing is considered as one of the most efficient methods for safety and security surveillance, with its adoption being continuously increased by many countries. Aerial views can provide better perspectives with the ability to cover large ground inaccessible areas and open seas. The adoption of such technology was mainly due to the fact that manned aircraft missions have been proved not so cost-effective and also potentially unsafe for the operators in extreme weather conditions [1]. On the contrary, Unmanned Aerial Vehicles (UAVs) function and operate at much lower costs with faster response times, providing safer ways for aerial remote surveillance [2].

UAVs are characterized mainly by their operational altitude and flight endurance, following existing military aerial platform classification [3]. Micro Aerial Vehicles (MAVs) operate at low altitudes ($< 330\ m$), while their small size limits battery capacities leading to their short flight times of approximately $5 - 30\ min$. These vehicles present significant potential and have been already used in real life missions for support of structure damage analysis [4] and rescue operations even in complex urban structure environments [5]. However, their Line-Of-Sight (LOS) operation limits their operational field in low scales. Medium Altitude, Long Endurance (MALE)

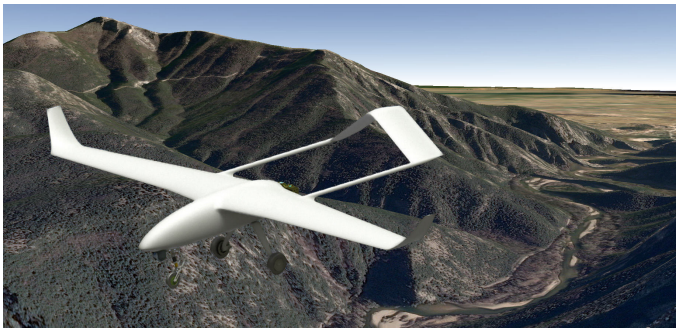

Fig. 1. HCUAV external geometry design.

aerial vehicles are much larger than MAVs classes, operating at altitudes approximately up to $9.000\ m$. Their flight time can last many hours, flying hundreds of kilometers away from their ground stations. The use of unmanned MALE platforms is appropriate when data collection is required at regional scales and can play significant role in strategic operations in defense and homeland security communities. Their usage in civil applications is also increased for long range communications or environmental and remote sensing [6]. Finally, the High Altitude, Long Endurance (HALE) class includes the largest and most complex aerial vehicles, with their size being similar to many general aviation manned aircrafts. These UAVs can fly at altitudes of $20.000\ m$ or more, on ranges that can be extended to thousands of kilometers with their flight duration reaching or exceeding 30 hours. This is the most recent class, being used for collecting information at global scales for climate variable assessments across broad regions of the globe. They can also support satellite observations at spatial and temporal scales [7]. However, the cost of such platforms is prohibitively expensive, thus they are used in large scale science campaigns, rather than smaller, localized operations where the other categories of UAVs platforms have been proved to be more cost effective.

The HCUAV project is aimed at developing a MALE UAV which tries to merge the superior characteristics of MAVs and HALEs. More precisely, low cost sensors and electronics will be combined with sophisticated image processing algorithms for delivering a cost efficient platform for accurate remote sensing and surveillance. This paper is focused on HCUAV's sensor payload and its supporting surveillance algorithms.

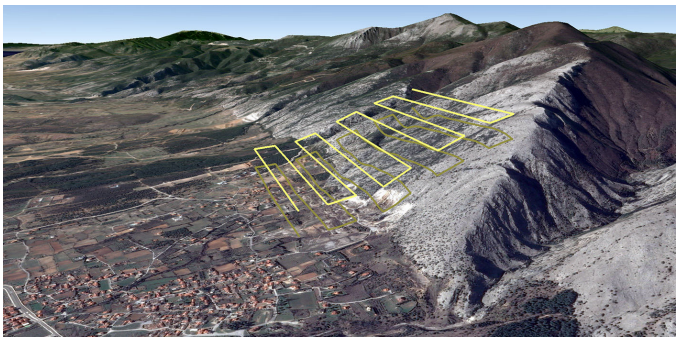

Fig. 2. Flight planning and altitude adjustment at loiter points for utilizing low cost sensors.

Preliminary simulation and experimental results for human activity, image mosaicking and fire detection show that low cost sensors on a MALE can work adequately in several mission operations.

II. HCUAV Framework

Structural and sensing requirements had to be defined considering the main operational objectives. Since the primary usage of HCUAV would be early forest fire detection and border control, the flight endurance, the range, the surveillance coverage and the flight velocities were adapted for such missions. Therefore, the demands in surveillance characteristics along with the unique terrain morphology lead to the defined requirements shown in Table I. Regarding the layout, a propeller-driven pusher configuration with a boom-mounted inverted V tail has been selected for the HCUAV, carrying an internal combustion engine as shown in Fig. 1.

HALEs typical mission profiles include only the three main segments of climbing, cruising and descending. The cruising altitude remains static and all remote sensing is performed at this level. Specifically, for performing image processing algorithms in such altitudes, application specific cameras are developed which are characterized by extremely high costs [8]. The geomorphology of the surveillance area in conjunction with the Above Ground Level (AGL) operation altitude as well as the requirements of the remote sensing algorithms result in the 3D mission path planning of Fig. 2, which differs from the flat cruising part of the HALEs surveillance operations.

Long-range communications will enable the data transfer between the platform and the ground control station. Data processing is divided between the ground and on-board processing units. Critical processing such as control [9], real-time warning information systems as well as image orthorectification, stitching and low computational cost (small-scale, low-accuracy) mosaicking are assigned to the on-board processing unit [10], [11]. However, more intensive image processing algorithms such as large-scale and high-accuracy stitching and mosaicking are performed in the ground station where there are no power or weight restrictions. The overall software architecture and the respective sensor data exchange are shown in Fig. 3.

III. HCUAV Sensor Payload

The UAV payload consists of an electro-optical and thermal sensor with resolution 1920×1080 and 640×480 pixels,

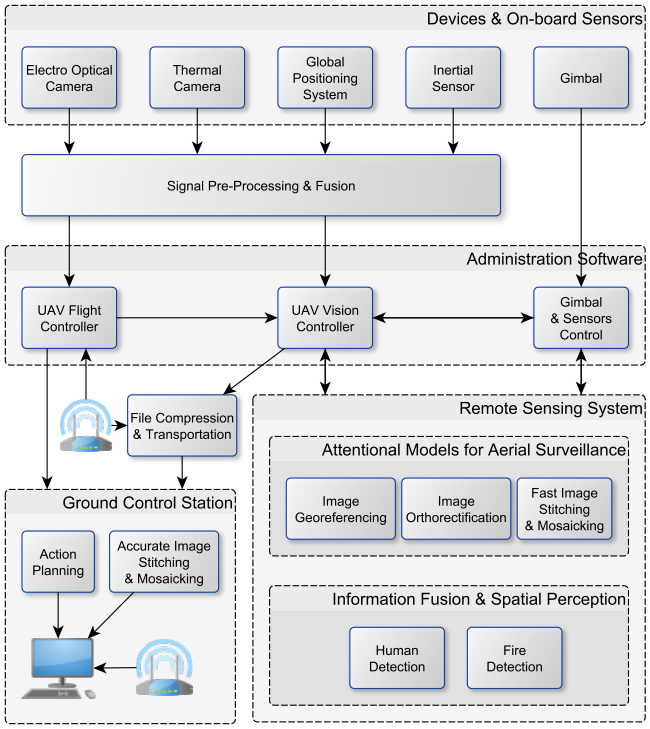

Fig. 3. HCUAV software architecture and sensor flowchart.

TABLE I. The HCUAV Requirements

Flight requirements	
Endurance	$> 8\ Hrs$
Loiter Velocity	$140\ km/h$
Maximum Velocity	$200\ km/h$
Operational Altitude	$2000\ m$
Structural requirements	
Payload Weight	$30\ kg$
Operating Temperature	$\leq 80^0 C$
Service Ceiling	$> 3\ km$
Sensor requirements	
Digital Camera	1920×1080
Thermal Camera	640×480
Global Positioning System	
Inertial Sensor	
Boundary Layer Sensors	

respectively, which are integrated into a gyro stabilized gimbal. The electro-optical sensor bears lens with 20x zoom capability [12], while the total weight of the equipment is less than 10 kg. The equipment is capable to survey both large areas in order to create proper maps and detect fires as well as small areas for human activity recognition. The Table II presents the Ground Sample Distance (GSD) and the footprint area for an indicative AGL altitude of 250m as well as for a variety of sensor pixel sizes and for two different focal lengths.

IV. HCUAV Remote Sensing Algorithms

The main purpose of the HCUAV project is to recognize human activity in border patrol missions, to detect fires at forested areas as well as to provide orthophotomaps. Thus,

TABLE II. GROUND SAMPLE DISTANCE FOR DIFFERENT SENSOR PIXEL SIZES AND FOCAL LENGTHS.

Sensor Resolution: 1920 Columns × 1080 Rows				
AGL Altitude: 250m				
Sensor pixel size [mm]	Focal Length: 5mm		Focal Length: 90mm	
	GSD [m]	Footprint Area [ha]	GSD [m]	Footprint Area [ha]
0.0025	0.125	3.2400	0.007	0.0100
0.0045	0.225	10.4976	0.013	0.0324
0.0065	0.325	21.9024	0.018	0.0676
0.0085	0.425	37.4544	0.024	0.1156
0.0105	0.525	57.1536	0.029	0.1764
0.0125	0.625	81.0000	0.035	0.2500
0.0145	0.725	108.9936	0.040	0.3364

the developed remote sensing algorithms are separated in two major categories: 1.image mosaicking and 2. human and fire detection. In order to accelerate the orthophotomaps creation, Digital Elevation Models (DEMs) of the surveillance area, which have been produced by a fusion process of other existing DEMs, are considered. Furthermore, the aforementioned 3D path planning process ensures properly shot aerial images.

A. DEMs Fusion

The process which is followed in order to create a fused DEM is consisted of four basic steps: 1. preprocessing, 2. forward transform of a spectral expansion method, 3. spectral coefficients fusion and finally, 4. inverse spectral transform in order to obtain the desired fused DEM. Since DEMs are 2D signals, separable basis functions like Fourier exponential function or Chebyshev [13] and Legendre [14] orthogonal polynomials may be used as kernel of the spectral expansion method. Regarding the 3^{rd} step, a weighted average of expansion coefficients is used.

B. Image Mosaicking

The image mosaicking process is separated into two main strategies: 1. fast, small-scale and low accuracy orthophotomaps creation, and 2. computationally demanding, large-scale and accurate orthophotomaps. The first strategy is conducted on-board in order to serve instantly as an initial, targeted reference map in emergency situations like forest fires, while the second one is performed on the ground control station in order to serve as a large area, detailed and accurate map for mission-oriented actions.

Having planned the UAV flight path and using the fused DEM, the first step in order to create an orthophotomap, is to perform image orthorectification and georeference. In the first strategy, a combination of forward image grid and backward DEM's grid projection in conjunction with GPS and inertial sensor data is used in order to attribute to each image pixel a value of height. Although this method strongly depends on the sensor and DEM accuracy, it is fast enough considering the project's requirements providing a georeferenced and orthorectified image, simultaneously. In the second strategy, a more sophisticated and computationally demanding algorithm, which includes feature detection, description, matching and homography calculation using RANSAC and image metadata for outliers removal, is applied to successive image pairs. In this process, elevation data are produced from the used image pairs in order to achieve image orthorectification. While this method is DEM independent, the fused DEM is used supportively for accuracy control. Utilizing the GPS and inertial sensor data, as well as the registered elevation data with the fused DEM, image georeferencing is calculated, as well.

Whenever two or more orthorectified and georeferenced images have been obtained, the image stitching process is initiated in order to create the mosaic which results in the desired orthophotomap. In the first strategy, this map is simply produced by considering the coordinates that have been attributed to each pixel of the image set during the georeference process. However, regarding the second strategy, a trade-off between the calculated image pixel coordinates and a homography transform should be considered in order to improve as much as possible the accuracy or the resulted map.

C. Human & Fire Detection

Taking into account the flight height, human and fire detection algorithms are mainly based on blob detection [15]. For both processes thermal radiation is taken into consideration, nevertheless, for the case of human recognition, information like movement as well as shadow size and shape are also considered.

Fire is relatively easy to be detected utilizing a proper blob detector (e.g. MSER [16]) in conjunction with a color based descriptor, applied to thermal and optical images, respectively. Unlike fire, human detection is a more demanding process resulting in a more sophisticated and complex algorithm. The main difficulty of human detection originates from the high flight altitude. The proposed algorithms are described by the following steps. Initially, a blob detector using a fused image, produced by an optical and thermal one, locates shadows and human-like blobs. Afterwards, a size filter is applied to shadow blobs in order to keep only objects with the size of a human. Subsequently, a matching process between shadow and human blobs takes place. Finally, any other information like object movement patterns is used supportively in order to increase the true positive recognition rate.

V. PRELIMINARY EXPERIMENTAL RESULTS

This Section presents the preliminary results of the HCUAV proposed algorithms. Since the UAV platform is under construction, we used real data area images from other UAV platforms and especially for human detection we utilized aerial images from Google Maps. Artificial worlds have been also used for evaluating the stitching and mosaicking performance.

A. DEM Fusion

Regarding the DEMs fusion, the studied geographic area, bounded according to longitude and latitude range: $[2^o24'00.0"W,\ 2^o25'48.0"W]$ and $[43^o18'00.0"N,\ 43^o19'48.0"N]$, respectively, has been selected due to

TABLE III. QUALITY MEASURES FOR DEMS RESULTED FROM FUSION PROCESSES WHICH ARE BASED ON DIFFERENT SPECTRAL EXPANSION METHODS.

Quality Measures	Spectral Methods		
	Chebyshev	Legendre	Fourier
Q	0.723	0.706	0.621
Q_w	0.724	0.719	0.659
Q_e	0.757	0.753	0.692
MI	0.607	0.603	0.599

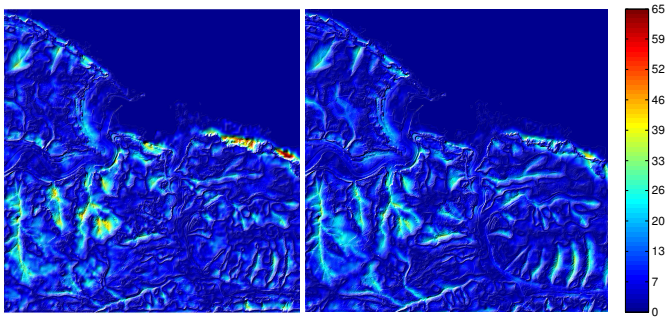

(a) (b)

Fig. 4. Square Error between (a) ASTER and (b) fused DEM produced by Chebyshev spectral method and lidar data (*The colorbar scale is in meters*).

the availability of lidar data[1] with 1m resolution, which can used as ground-truth basis for error calculation. In order to produce the fused DEM which is going to be used to the orthophotomaps creation, two free DEMs, the SRTM [17] and ASTER [18] are used as inputs into the fusion process.

Mutual Information [19] as well as Piella's metrics (Q, Q_w, $Q_e(\alpha) \in [-1, 1]$) [20] are very useful for evaluating the fusion process. The closer the value of above measures to 1, the better the quality of the fused DEM. Table III presents the values of the quality measures for DEMs resulted from fusion processes which are based on different spectral expansion methods (Chebyshev, Fourier, Legendre). It can be seen that the Chebyshev spectral method in conjunction with the aforementioned weighting average fusion process of expansion coefficients, leads to the best fused DEM.

Fig. 4(a) illustrates the Square Error between ASTER DEM and the lidar data, while Fig. 4(b) presents the Square Error between lidar data and the fused DEM produced by Chebyshev spectral method. By examining the performance results, it can be concluded that the proposed fused DEM is characterized by lower error (max ASTER error: 65m, max fused DEM error 42m) and thus, by more accurate elevation values.

B. Image Stitching-Mosaicking

At this point it should be noted that only the fast, small-scale mosaicking process has been developed so far. By examining Fig. 5, it can be concluded that the developed algorithm perform well for the examined artificial world, producing outputs close enough to the ground truth orthorectified image.

[1] http://b5m.gipuzkoa.net/

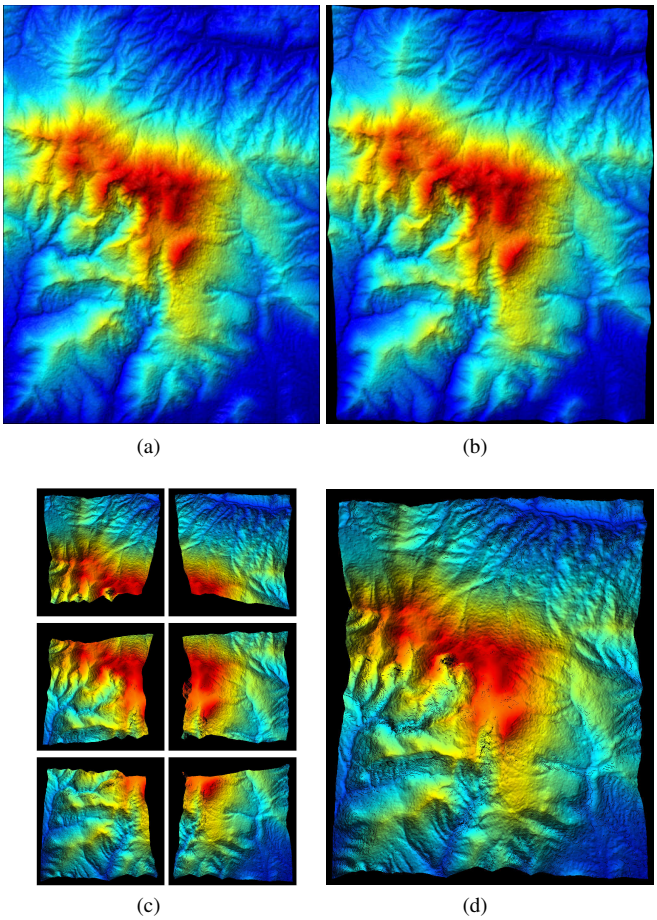

(a) (b) (c) (d)

Fig. 5. Image mosaicking: (a) ground truth orthorectified image, (b) camera perspective view, (c) individual orthorectified images, (d) mosaic.

The used artificial world has been created in MATLAB Mapping Toolbox, where the illustrated geographic area has latitude and longitude range, [41.195596, 41.370461] and [24.020735, 24.186855], respectively. The viewpoint of the camera images are characterized by 80% forward and 60% side overlap.

C. Human & Fire Detection

As mentioned in Section IV, for human and fire detection, images from both electro-optical and thermal sensors are considered. Figures 6(a-b) and 6(c-d), illustrate the qualitatively results of human and fire detection, respectively. Unlike human detection where false positive and false negative results may be seen, the fire detection algorithm performs adequately.

VI. CONCLUSION AND FUTURE WORK

The paper presented the overall framework and on-going research activity of the security related project HCUAV focused on developing a MALE UAV equipped with low cost remote sensing instrumentations for performing civilian operations. The sensor and algorithm research targets specifically at recognizing human activity in border patrol missions, detecting

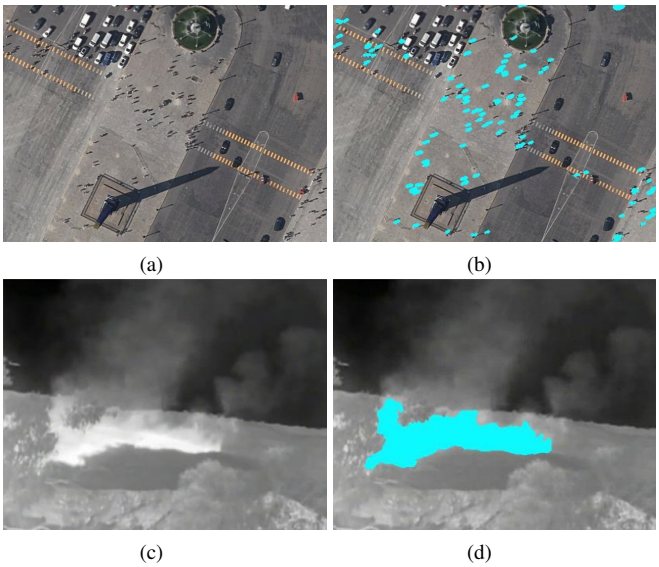

Fig. 6. Results from human & fire detection algorithms: (a-b) Urban area human detection, (c-d) fire detection using thermal imaging.

fires at forested areas as well providing orthorectified aerial images. Preliminary experimental results show the effectiveness of the proposed sensor and algorithm architecture in medium altitude remote sensing applications.

Future trials will examine the software and sensor effectiveness in real missions where numerous issues such as weather conditions and platform oscillations will be also evaluated. Human activity in non-urban areas, and large scale image stitching based on probabilistic models are also areas for future consideration. Finally, a trade-off between sensory cost effectiveness and loitering fuel cost and consumption will be evaluated for accurate verification of the proposed software and sensor architecture.

ACKNOWLEDGMENT

The work presented in this paper is part of the 11SYNERGASIA_9_629 "Hellenic Civil Unmanned Air Vehicle - HCUAV" research project, implemented within the framework of the National Strategic Reference Framework (NSRF) and through the Operation Programme "Competitiveness & Entrepreneurship – SYNERGASIA 2011". The research project is co-financed by National and Community Funds, 25% from the Greek Ministry of Education and Religious Affairs - General Secretariat of Research and Technology and 75% from E.U. - European Social Fund.

REFERENCES

[1] J. M. Peschel and R. R. Murphy, "On the human–machine interaction of unmanned aerial system mission specialists," *IEEE Transactions on Human-Machine Systems*, vol. 43, no. 1, pp. 53–62, 2013.

[2] B. Siciliano and O. Khatib, *Springer handbook of robotics*. Springer, 2008.

[3] A. C. Watts, V. G. Ambrosia, and E. A. Hinkley, "Unmanned aircraft systems in remote sensing and scientific research: Classification and considerations of use," *Remote Sensing*, vol. 4, no. 6, pp. 1671–1692, 2012.

[4] N. Michael, S. Shen, K. Mohta, Y. Mulgaonkar, V. Kumar, K. Nagatani, Y. Okada, S. Kiribayashi, K. Otake, K. Yoshida, K. Ohno, E. Takeuchi, and S. Tadokoro, "Collaborative mapping of an earthquake-damaged building via ground and aerial robots," *Journal of Field Robotics*, vol. 29, no. 5, pp. 832–841, 2012.

[5] M. Achtelik, Y. Brunet, M. Chli, S. Chatzichristofis, J. Decotignie, K. Doth, F. Fraundorfer, L. Kneip, D. Gurdan, L. Heng, E. Kosmatopoulos, L. Doitsidis, G. H. Lee, S. Lynen, A. Martinelli, L. Meier, M. Pollefeys, D. Piguet, A. Renzaglia, D. Scaramuzza, R. Siegwart, J. Stumpf, P. Tanskanen, C. Troiani, and S. Weiss, "Sfly: Swarm of micro flying robots," in *IEEE/RSJ International Conference on Intelligent Robots and Systems*, 2012, pp. 2649–2650.

[6] M. Fladeland, M. Sumich, B. Lobitz, R. Kolyer, D. Herlth, R. Berthold, D. McKinnon, L. Monforton, J. Brass, and G. Bland, "The nasa sierra science demonstration programme and the role of small–medium unmanned aircraft for earth science investigations," *Geocarto International*, vol. 26, no. 2, pp. 157–163, 2011.

[7] L. Marconi, C. Melchiorri, M. Beetz, D. Pangercic, R. Siegwart, S. Leutenegger, R. Carloni, S. Stramigioli, H. Bruyninckx, P. Doherty, A. Kleiner, V. Lippiello, A. Finzi, B. Siciliano, A. Sala, and N. Tomatis, "The sherpa project: smart collaboration between humans and ground-aerial robots for improving rescuing activities in alpine environments," in *IEEE International Symposium on Safety, Security, and Rescue Robotics*, 2012, pp. 1–4.

[8] T. Van Achteren, B. Delauré, J. Everaerts, D. Beghuin, and R. Ligot, "Medusa: an ultra-lightweight multi-spectral camera for a hale uav," in *Remote Sensing*, 2007, pp. 67 441P–67 441P.

[9] Y. Liang, Y. Jia, and F. Matsuno, "A fault-tolerant integrated navigation for uav systems using time-variant vector distribution coefficients," in *American Control Conference*, 2014, pp. 678–683.

[10] A. Amanatiadis, A. Gasteratos, C. Georgoulas, L. Kotoulas, and I. Andreadis, "Development of a stereo vision system for remotely operated robots: A control and video streaming architecture," in *IEEE International Conference on Virtual Environments, Human-Computer Interfaces and Measurement Systems*, 2008, pp. 14–19.

[11] A. Amanatiadis, L. Bampis, and A. Gasteratos, "Accelerating image super-resolution regression by a hybrid implementation in mobile devices," in *IEEE International Conference on Consumer Electronics*, 2014, pp. 335–336.

[12] A. Amanatiadis and I. Andreadis, "An integrated architecture for adaptive image stabilization in zooming operation," *IEEE Transactions on Consumer Electronics*, vol. 54, no. 2, pp. 600–608, 2008.

[13] Z. Omar, N. Mitianoudis, and T. Stathaki, "Two-dimensional chebyshev polynomials for image fusion," in *28th Picture Coding Symposium*, 2010, pp. 426–429.

[14] E. Karakasis, G. Papakostas, D. Koulouriotis, and V. Tourassis, "A unified methodology for computing accurate quaternion color moments and moment invariants," *IEEE Transactions on Image Processing*, vol. 23, no. 2, pp. 596–611, 2014.

[15] V. Reilly, B. Solmaz, and M. Shah, "Geometric constraints for human detection in aerial imagery," in *European Conference on Computer Vision*, 2010, pp. 252–265.

[16] J. Matas, O. Chum, M. Urban, and T. Pajdla, "Robust wide-baseline stereo from maximally stable extremal regions," *Image and vision computing*, vol. 22, no. 10, pp. 761–767, 2004.

[17] T. Farr, P. Rosen, E. Caro, R. Crippen, R. Duren, S. Hensley, M. Kobrick, M. Paller, E. Rodriguez, L. Roth, D. Seal, S. Shaffer, J. Shimada, J. Umland, M. Werner, M. Oskin, D. Burbank, and D. Alsdorf, "The shuttle radar topography mission," *Reviews of Geophysics*, vol. 45, no. 2, 2007.

[18] H. Reuter, A. Nelson, P. Strobl, W. Mehl, and A. Jarvis, "A first assessment of aster gdem tiles for absolute accuracy, relative accuracy and terrain parameters," in *IEEE International Geoscience and Remote Sensing Symposium*, vol. 5, 2009, pp. V240–V243.

[19] G. Qu, D. Zhang, and P. Yan, "Information measure for performance of image fusion," *Electronics Letters*, vol. 38, no. 7, pp. 313–315, 2002.

[20] G. Piella, "New quality measures for image fusion," in *Proceedings of the Seventh International Conference on Information Fusion*, vol. 1, 2004, pp. 542–546.